ACADEMIC PRESS

Available online at www.sciencedirect.com
SCIENCE DIRECT®

Journal of Colloid and Interface Science 264 (2003) 335–342

JOURNAL OF Colloid and Interface Science

www.elsevier.com/locate/jcis

Analytical investigation of two-step adsorption kinetics on surfaces

Hiroki Nagaoka [a] and Toyoko Imae [a,b,*]

[a] *Faculty of Science, Nagoya University, Nagoya 464-8602, Japan*
[b] *Research Center for Materials Science, Nagoya University, Nagoya 464-8602, Japan*

Received 10 January 2003; accepted 21 March 2003

Abstract

Analytical equations of two-step adsorption kinetics on surface have been derived. Moreover, computer simulations have been carried out to interpret various experimental adsorption kinetics previously reported. In the first case, molecules are further adsorbed from a solution onto a layer consisting of previously adsorbed molecules. This model was applied to the adsorption kinetics of hexadecyltrimethylammonium chloride (C_{16}TAC) on a self-assembled monolayer (SAM) of 3-mercaptopropionic acid (T. Imae, H. Torii, J. Phys. Chem. B 104 (2000) 9218). The second case is that some of the initially adsorbed molecules are released from the adlayer with further time course. The adsorption of C_{16}TAC on 1-dodecanethiol SAM (T. Imae, T. Takeshita, K. Yahagi, Stud. Surf. Sci. Catal. 132 (2001) 477) agrees with this mechanism. The strict mathematical developments presented in this work are demanded to specify the physical meaning of observed non-Langmuir adsorption kinetics, consisting of the two exponential terms.
© 2003 Elsevier Inc. All rights reserved.

Keywords: Two-step adsorption kinetics; Langmuir adsorption kinetics; Hexadecyltrimethylammonium chloride; 3-Mercaptopropionic acid; 1-Dodecanethiol; Self-assembled monolayer

1. Introduction

The recent development of analytical methodological techniques allows quantitatively investigation of the adsorption kinetics of tiny numbers of molecules. Ellipsometry [1–6], quartz crystal microbalance (QCM) [7–13], surface plasmon resonance (SPR) spectroscopy [14–23], reflectometry [24,25], atomic force microscopy [26,27], temperature-programmed desorption spectroscopy [28], potentiostat [29], attenuated total reflection (ATR)-infrared absorption spectroscopy [30], and ATR-surface enhanced infrared absorption (SEIRA) spectroscopy [23,31] have been used for the investigation of the adsorption kinetics of molecules on substrates [1–4,6–11,13,14,21,22,24–31] and on self-assembled monolayers (SAM) [5,10,12,15–20,23,31].

Various adsorption models have been developed to analyze the observed kinetics. From these studies, it has been shown that simple Langmuir (monolayer) adsorption kinetics interprets the formation of thiol SAMs on metals [2,7–9, 11,31]. However, profiles of some other experimental kinetics do not obey the simple Langmuir adsorption equation. Adsorption by a two-step process has been reported for the formation of thiol SAM [1,9,26]. The process proceeds by initial fast adsorption and a subsequent slow step. Hu and Bard [26] have explained this process by the repulsive interaction between adsorbed ionic thiols. Garg et al. [3], Xu et al. [27], and Lavrich et al. [28] have suggested the transition from physisorption to chemisorption for thiol on gold surfaces. Peterlinz and Georgiadis [14] have reported thiol adsorption, which was described by a series of up to three steps of distinct kinetics. They analyzed this kinetics on the basis of the diffusion-limited first-order Langmuir model and the second-order non-diffusion-limited model.

The kinetics profiles of molecular adsorption have also been discussed for other systems than SAM formation. Takada et al. [29] have reported that dendrimer adsorption onto Pt electrode obeys Langmuir adsorption kinetics. Schouten et al. [17] have modeled the kinetics of DNA adsorption on cationic lipids using the Langmuir equation. In this case, it was argued that the adsorption kinetics of molecules on SAM strongly depends on the SAM composition [15,17] and is affected by additional effects [16]. On the other hand, for the adsorption process of glucosylated poly(phenylisocyanide) on hydrophilic surfaces, Hasegawa et al. [12] have reported that the initial rapid decrease of

* Corresponding author.
E-mail address: imae@nano.chem.nagoya-u.ac.jp (T. Imae).

0021-9797/$ – see front matter © 2003 Elsevier Inc. All rights reserved.
doi:10.1016/S0021-9797(03)00314-X

the QCM frequency was gradually converted to a slow monotonic decrease. They applied an analytical kinetics equation with a first term corresponding to first-layer adsorption and a second term due to subsequent multiadsorption. This is in contrast to a case reported for poly(glycostyrene) adsorbed on hydrophobic surfaces, which was interpreted according to Langmuir kinetics without multilayers [10].

One of the present authors (T.I.) and her collaborators [23,31] have investigated the adsorption kinetics of hexadecyltrimethylammonium chloride (C_{16}TAC) on thiol SAM. It was concluded that the adsorption of C_{16}TAC on hydrophilic 3-mercapto-1-propanol SAM proceeds according to the Langmuir equation [23]. On the other hand, the adsorption of C_{16}TAC on hydrophilic 3-mercaptopropionic acid (MPA) SAM has fast adsorption at early stages and slow adsorption at later times [31]. The transition of carboxylic acid to carboxylate was proved by ATR-SEIRA spectroscopy, indicating the formation of ion-pairs of C_{16}TAC with MPA SAM by electrostatic interaction. In this case, a second adsorption layer of C_{16}TAC must be considered, since the hydrophobic first adsorption layer faces the bulk water. This is the origin of the two-step mechanism in the case of C_{16}TAC adsorption on MPA SAM. In contrast, the adsorption of C_{16}TAC on hydrophobic 1-dodecanethiol SAM at C_{16}TAC concentrations below the critical micelle concentration displays initial excess adsorption amount. Excess adsorbed molecules are desorbed and rearranged to monolayer adsorption state [23]. Although these adsorption mechanisms were qualitatively explained, they could not be quantitatively interpreted by the available kinetics equations.

In the current paper, we derive new analytical equations for two-step adsorption kinetics and apply them to the analysis of the observed kinetics reported before [23,31]. Two adsorption mechanisms are considered: one where molecules form a monolayer and adsorb on the monolayer, and one where excess molecules adsorbed at an early stage are released to form a monolayer. The analytical curves of the kinetics were calculated, and computer simulations were carried out to interpret the experimental data of C_{16}TAC adsorption on SAMs.

2. Adsorption kinetics

2.1. Langmuir monolayer adsorption kinetics

We suppose that all adsorption sites S are equivalent and independent of the occupation of neighboring sites in the Langmuir monolayer adsorption of an adsorbate A, which is expressed by

$$\mathrm{A} + \mathrm{S} \underset{k_d}{\overset{k_a}{\rightleftharpoons}} \mathrm{A\text{–}S}. \tag{2.1}$$

The rate at which surface coverage changes during the adsorption and desorption processes depends on the concentration C of the adsorbate A in the solution and the numbers of occupied and nonoccupied adsorption sites, N_1 and $(N - N_1)$, respectively, where N is the total number of adsorption sites. If k_a and k_d are the intrinsic rate constants of adsorption and desorption, respectively, the rate equation at a finite time t is described by

$$\frac{dN_1}{dt} = k_a C(N - N_1) - k_d N_1. \tag{2.2}$$

After integration,

$$\frac{N_1}{N} = I\left\{1 - \exp(-k_{\mathrm{obs}} t)\right\} \tag{2.3}$$

where

$$I = \frac{k_a C}{k_{\mathrm{obs}}}, \tag{2.4}$$

$$k_{\mathrm{obs}} = k_a C + k_d. \tag{2.5}$$

Relations (2.3)–(2.5) correspond to the well-known Langmuir adsorption kinetics equation [8].

2.2. Two-step adsorption kinetics

2.2.1. Formation of monolayer and additional adsorption on it

We assume that a first layer is formed on the adsorption sites S, and, in turn, a second layer is piled up on the first layer, as illustrated in Fig. 1. Thus, the adsorption reaction of adsorbate A is described by

$$\mathrm{A} + \mathrm{S} \underset{k_d}{\overset{k_a}{\rightleftharpoons}} \mathrm{A\text{–}S}, \tag{2.6}$$

$$\mathrm{A} + \mathrm{A\text{–}S} \underset{k'_d}{\overset{k'_a}{\rightleftharpoons}} \mathrm{AA\text{–}S}. \tag{2.7}$$

If N is the total number of adsorption sites, and N_1 and N_2 are the numbers of adsorption sites occupied in the first and second layers, respectively, then $N \geqslant N_1 \geqslant N_2$. If the rate constants of adsorption and desorption of the first layer

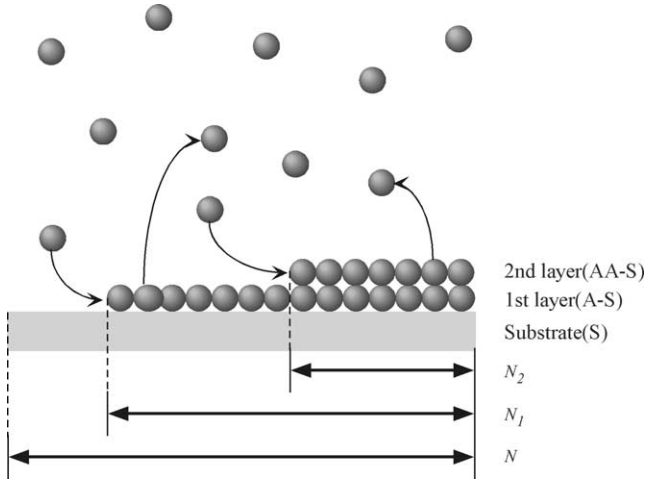

Fig. 1. Schematic representation of adsorption mechanism consisting of the first and second adlayers. N, total number of adsorption sites; N_1, number of occupied sites at first layer; N_2, number of occupied sites at second layer.

are denoted by k_a and k_d, respectively, and those corresponding to the second layer are denoted by k'_a and k'_d, the rate equations for an adsorbate concentration C can be written as

$$\frac{dN_1}{dt} = k_a C(N - N_1) - k_d(N_1 - N_2) = k_a CN - (k_a C + k_d)N_1 + k_d N_2, \quad (2.8)$$

$$\frac{dN_2}{dt} = k'_a C(N_1 - N_2) - k'_d N_2 = k'_a CN_1 - (k'_a C + k'_d)N_2. \quad (2.9)$$

Integrating for the initial condition $N_{1,0} = N_{2,0} = 0$ at $t = 0$,

$$\frac{N_1}{N} = \frac{\gamma\delta}{k_{1,\mathrm{obs}}k_{2,\mathrm{obs}}} + \frac{\delta}{k_{1,\mathrm{obs}} - k_{2,\mathrm{obs}}} \times \left\{ \frac{\gamma - k_{1,\mathrm{obs}}}{k_{1,\mathrm{obs}}} \exp(-k_{1,\mathrm{obs}}t) - \frac{\gamma - k_{2,\mathrm{obs}}}{k_{2,\mathrm{obs}}} \exp(-k_{2,\mathrm{obs}}t) \right\}, \quad (2.10)$$

$$\frac{N_2}{N} = \frac{\delta\delta'}{k_{1,\mathrm{obs}}k_{2,\mathrm{obs}}} + \frac{\delta}{k_{1,\mathrm{obs}} - k_{2,\mathrm{obs}}} \times \left\{ \frac{\delta'}{k_{1,\mathrm{obs}}} \exp(-k_{1,\mathrm{obs}}t) - \frac{\delta'}{k_{2,\mathrm{obs}}} \exp(-k_{2,\mathrm{obs}}t) \right\} \quad (2.11)$$

(see Appendix A and B), and

$$\frac{N_1 + N_2}{N} = I_1\{1 - \exp(-k_{1,\mathrm{obs}}t)\} + I_2\{1 - \exp(-k_{2,\mathrm{obs}}t)\}, \quad (2.12)$$

where

$$I_1 = \frac{-\delta}{k_{1,\mathrm{obs}} - k_{2,\mathrm{obs}}} \frac{\gamma + \delta' - k_{1,\mathrm{obs}}}{k_{1,\mathrm{obs}}},$$

$$I_2 = \frac{\delta}{k_{1,\mathrm{obs}} - k_{2,\mathrm{obs}}} \frac{\gamma + \delta' - k_{2,\mathrm{obs}}}{k_{2,\mathrm{obs}}},$$

$$k_{1,\mathrm{obs}} = \alpha + \sqrt{\alpha^2 - \beta^2},$$

$$k_{2,\mathrm{obs}} = \alpha - \sqrt{\alpha^2 - \beta^2}, \quad (2.13)$$

and

$$2\alpha = k_a C + k_d + k'_a C + k'_d,$$

$$\beta^2 = k_a k'_a C^2 + k_a k'_d C + k_d k'_d,$$

$$\gamma = k'_a C + k'_d,$$

$$\delta = k_a C,$$

$$\delta' = k'_a C. \quad (2.14)$$

According to Eqs. (2.10) and (2.11), if $k'_a \to 0$ and $k'_d \to 0$ (Langmuir adsorption),

$$\frac{N_1}{N} = \frac{k_a C}{k_a C + k_d}\left[1 - \exp\{-(k_a C + k_d)t\}\right] \quad (2.15)$$

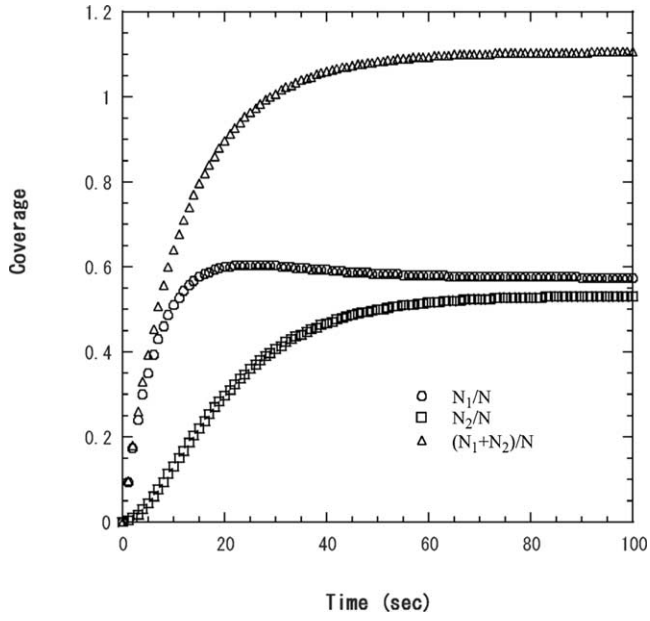

Fig. 2. A model calculation of the mechanism in Fig. 1 using the parameters $k_a = 0.01\ \mathrm{M^{-1}\,s^{-1}}$, $k_d = 0.05\ \mathrm{s^{-1}}$, $k'_a = 0.005\ \mathrm{M^{-1}\,s^{-1}}$, $k'_d = 0.004\ \mathrm{s^{-1}}$, and $C = 10$ M. (○) N_1/N; (□) N_2/N; (△) $(N_1 + N_2)/N$.

and

$$\frac{N_2}{N} = 0. \quad (2.16)$$

It can be seen that the relations (2.15) and (2.16) are consistent with Eq. (2.3) derived for the Langmuir adsorption.

Figure 2 shows a profile of the adsorption kinetics computed from Eqs. (2.10)–(2.12) with parameters $k_a = 0.01\ \mathrm{M^{-1}\,s^{-1}}$, $k_d = 0.05\ \mathrm{s^{-1}}$, $k'_a = 0.005\ \mathrm{M^{-1}\,s^{-1}}$, $k'_d = 0.004\ \mathrm{s^{-1}}$, and $C = 10$ M. While the first layer adsorption provided by the parameter N_1/N is saturated at an early stage of the adsorption, the second layer adsorption (N_2/N) increases gradually with adsorption time. Therefore, the contribution of the first layer adsorption occurs mainly at the initial steep increase in the total coverage ($(N_1 + N_2)/N$) in which the second layer adsorption is slow. Even if k_a is increased one order of magnitude and k'_a and k'_d are decreased by the same amount, the common profile of the kinetics curve is maintained, as can be seen in Fig. 3. However, in this case, the first layer adsorption is achieved at an earlier adsorption time than in the case in Fig. 2.

2.2.2. Desorption and rearrangement of molecules in the adlayer

We assume that many molecules are adsorbed at an initial stage and that they can then be rearranged to form a monolayer. Since a monolayer can be formed in the equilibrium state, excess molecules must be desorbed during the rearrangement to the monolayer, as illustrated in Fig. 4. This mechanism can be written as

$$n\mathrm{A} + \mathrm{S} \underset{k_d}{\overset{k_a}{\rightleftharpoons}} n\mathrm{A_p}\text{–}\mathrm{S}, \quad (2.17)$$

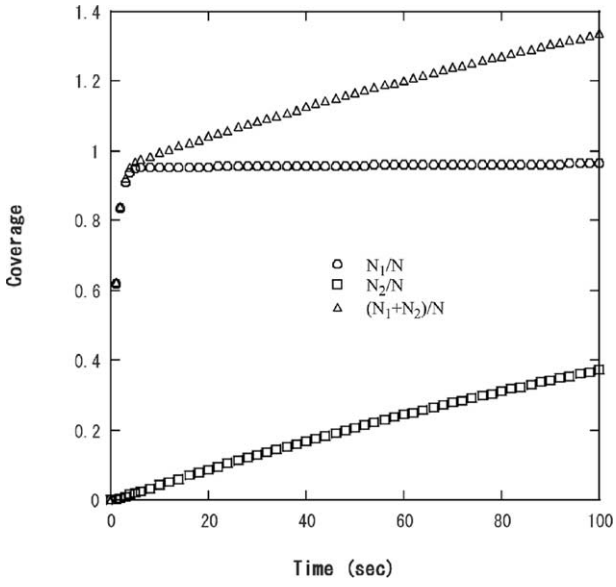

Fig. 3. A model calculation of the mechanism in Fig. 1 using the parameters $k_a = 0.1\ \mathrm{M^{-1}\,s^{-1}}$, $k_d = 0.05\ \mathrm{s^{-1}}$, $k'_a = 0.0005\ \mathrm{M^{-1}\,s^{-1}}$, $k'_d = 0.0001\ \mathrm{s^{-1}}$, and $C = 10$ M. (○) N_1/N; (□) N_2/N; (△) $(N_1 + N_2)/N$.

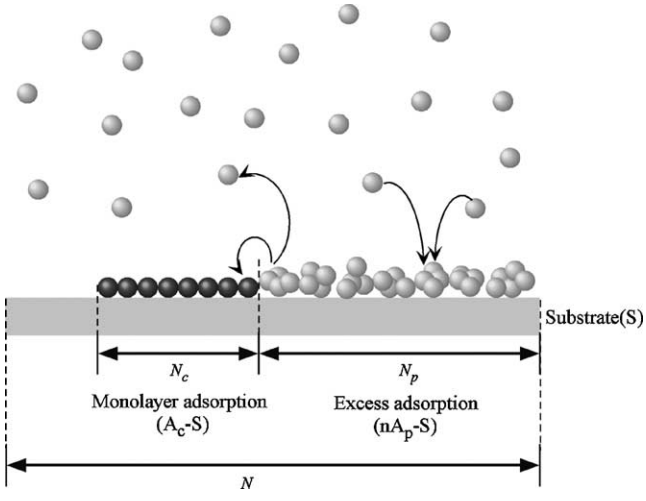

Fig. 4. Schematic representation of the mechanism transferring from excess adsorption to monolayer adsorption. N, total number of adsorption sites; N_p, number of sites occupied by excess adsorption; N_c, number of sites occupied by monolayer adsorption.

$$n\mathrm{A_p{-}S} \xrightarrow{k_t} \mathrm{A_c{-}S} + (n-1)\mathrm{A}, \tag{2.18}$$

where A represents the adsorbate and n is the hypothetical member of adsorbates per adsorption site S. A_p represents the initially adsorbed species and A_c is a species rearranged into monolayer. If k_a and k_d denote the rate constants of Eq. (2.17) for adsorption and desorption, respectively, and k_t is the rate constant of Eq. (2.18), then the adsorption rate equations at a time t can be deduced for an arbitrary adsorbate concentration C as

$$\begin{aligned}\frac{dN_p}{dt} &= k_a C\{N - (N_p + N_c)\} - k_d N_p - k_t N_p \\ &= k_a C N - (k_a C + k_d + k_t)N_p - k_a C N_c\end{aligned} \tag{2.19}$$

and

$$\frac{dN_c}{dt} = k_t N_p, \tag{2.20}$$

where N is the total number of adsorption sites, and N_p and N_c are the number of occupied sites initially and in the monolayer, respectively. Eqs. (2.19) and (2.20) were integrated by means of a procedure similar to the integration of Eqs. (2.8) and (2.9). Then

$$\frac{N_p}{N} = \frac{-\eta}{k'_{1,\mathrm{obs}} - k'_{2,\mathrm{obs}}}\left\{\exp(-k'_{1,\mathrm{obs}}t) - \exp(-k'_{2,\mathrm{obs}}t)\right\}, \tag{2.21}$$

$$\begin{aligned}\frac{N_c}{N} = \frac{-\eta}{k'_{1,\mathrm{obs}} - k'_{2,\mathrm{obs}}}\Bigg[&\frac{\eta'}{k'_{1,\mathrm{obs}}}\left\{1 - \exp(-k'_{1,\mathrm{obs}}t)\right\} \\ &- \frac{\eta'}{k'_{2,\mathrm{obs}}}\left\{1 - \exp(-k'_{2,\mathrm{obs}}t)\right\}\Bigg],\end{aligned} \tag{2.22}$$

and

$$\begin{aligned}\frac{nN_p + N_c}{N} = {}& I'_1\left\{1 - \exp(-k'_{1,\mathrm{obs}}t)\right\} \\ &+ I'_2\left\{1 - \exp(-k'_{2,\mathrm{obs}}t)\right\},\end{aligned} \tag{2.23}$$

where

$$\begin{aligned}I'_1 &= \frac{-\eta}{k'_{1,\mathrm{obs}} - k'_{2,\mathrm{obs}}}\frac{\eta' - nk'_{1,\mathrm{obs}}}{k'_{1,\mathrm{obs}}}, \\ I'_2 &= \frac{\eta}{k'_{1,\mathrm{obs}} - k'_{2,\mathrm{obs}}}\frac{\eta' - nk'_{2,\mathrm{obs}}}{k'_{2,\mathrm{obs}}}, \\ k'_{1,\mathrm{obs}} &= \varepsilon + \sqrt{\varepsilon^2 - \phi^2}, \\ k'_{2,\mathrm{obs}} &= \varepsilon - \sqrt{\varepsilon^2 - \phi^2},\end{aligned} \tag{2.24}$$

and

$$\begin{aligned}&2\varepsilon = k_a C + k_d + k_t, \qquad \phi^2 = k_a k_t C, \\ &\eta = k_a C, \qquad \eta' = k_t.\end{aligned} \tag{2.25}$$

The coverage was calculated from Eqs. (2.21)–(2.23) by using the parameters $k_a = 0.5\ \mathrm{M^{-1}\,s^{-1}}$, $k_d = 0.1\ \mathrm{s^{-1}}$, $k_t = 0.05\ \mathrm{s^{-1}}$, $C = 1$ M, and $n = 1$ to 2. As seen in Fig. 5, the coverage at the initial adsorption step increases sharply at the initial stage of adsorption but they decreases with the rearrangement into monolayer. For an initial adsorption at $n = 1$, the total surface coverage displays initial sharp increase and gradual increase. The profile of total coverage changes with the value of n and shows a maximum at the initial adsorption stage and a decrease at long times for high n values ($n > 1.2$). These results clearly indicate that the adsorption profile changes depending on the contribution of the initial adlayer.

3. C_{16}TAC adsorption on SAMs

The adsorption kinetics of C_{16}TAC from a 0.1 wt% solution on MPA SAM has been investigated by ATR SEIRA

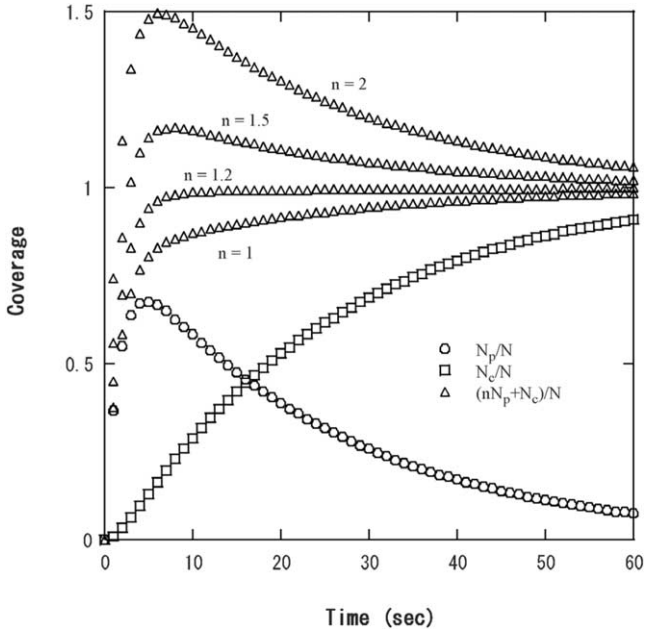

Fig. 5. A model calculation of the mechanism in Fig. 4 using the parameters $k_a = 0.5\ \mathrm{M^{-1}\ s^{-1}}$, $k_d = 0.1\ \mathrm{s^{-1}}$, $k_t = 0.05\ \mathrm{s^{-1}}$, $C = 1$ M, and $n = 1$ to 2. (○) N_p/N; (□) N_c/N; (△) $(nN_p + N_c)/N$.

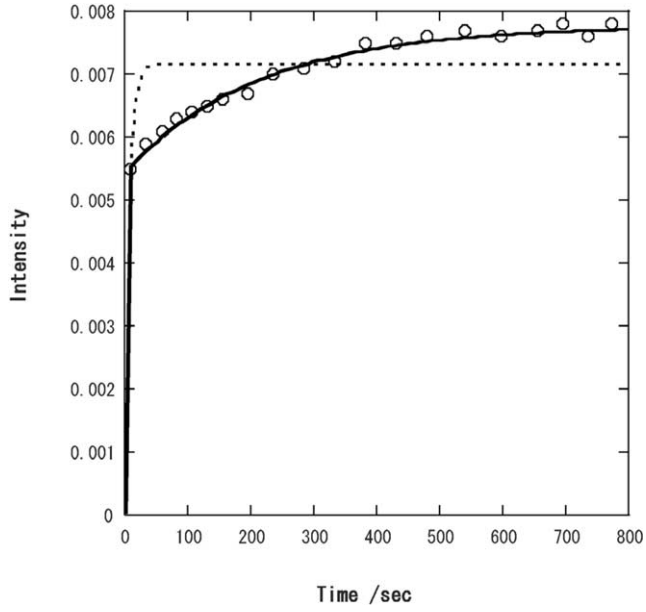

Fig. 6. Intensity increase of a CH_2 antisymmetric stretching vibration band as a function of adsorption time for C_{16}TAC adsorption from an aqueous 0.1 wt% solution on MPA SAM [31] and the corresponding computer simulation. Open circle, obs; broken line, the curve calculated from Eq. (3.1), on the basis of the Langmuir monolayer adsorption mechanism, with $I_{\mathrm{int}} = 0.0072$ and $k_{\mathrm{obs}} = 0.14\ \mathrm{s^{-1}}$ (correlation coefficient 0.508); solid line, the curve calculated from Eq. (3.2), on the basis of the mechanism in Fig. 1, with $I_{\mathrm{int},1} = -0.0023$, $k_{1,\mathrm{obs}} = 0.0047\ \mathrm{s^{-1}}$, $I_{\mathrm{int},2} = 0.0054$, and $k_{2,\mathrm{obs}} = 0.50\ \mathrm{s^{-1}}$ (correlation coefficient 0.991).

spectroscopy [31]. It was observed on the time course of adsorption of C_{16}TAC that the intensity of the CH_2 antisymmetric stretching vibration band increased sharply within 20 s and then gradually up to ∼800 s. Since the C_{16}TA cation makes an ion-pair with the deprotonated MPA SAM, the adsorption of C_{16}TAC on MPA SAM must be fundamentally monolayer adsorption. However, the intensity increase cannot be explained by the Langmuir monolayer adsorption kinetics equation, as seen in Fig. 6, where the equation

$$I_{\mathrm{int}} = I_{\mathrm{int},\infty}\left\{1 - \exp(-k_{\mathrm{obs}}t)\right\} \tag{3.1}$$

with the parameters $I_{\mathrm{int},\infty} = 0.0072$ and $k_{\mathrm{obs}} = 0.14\ \mathrm{s^{-1}}$ was used instead of Eq. (2.3). I_{int} is the observed SEIRA intensity and $I_{\mathrm{int},\infty}$is the intensity at $t = \infty$. Then, additional adsorption of C_{16}TAC onto the C_{16}TAC monolayer on MPA SAM was considered. The computer simulation was performed using an equation analogous to Eq. (2.12):

$$I_{\mathrm{int}} = I_{\mathrm{int},1}\left\{1 - \exp(-k_{1,\mathrm{obs}}t)\right\} + I_{\mathrm{int},2}\left\{1 - \exp(-k_{2,\mathrm{obs}}t)\right\}. \tag{3.2}$$

As shown in Fig. 6, good agreement with the observed curve was obtained for the parameters $I_{\mathrm{int},1} = -0.0023$, $k_{1,\mathrm{obs}} = 0.0047\ \mathrm{s^{-1}}$, $I_{\mathrm{int},2} = 0.0054$, and $k_{2,\mathrm{obs}} = 0.50\ \mathrm{s^{-1}}$. Assuming that the amount adsorbed at the monolayer coverage is close to the transition point from sharp increase to slow one in the intensity, as it is the case shown in Fig. 3, the total adsorption amount of C_{16}TAC that can be deduced from Fig. 6 is 1.37 times more than the adsorption amount at the monolayer coverage.

It was observed by SPR spectroscopy that the resonance angle shift profile for a 0.1 wt% solution of C_{16}TAC on MPA SAM reached a constant value (∼0.025°) at the equilibrium state [32]. The adsorption thickness of C_{16}TAC calculated from the shift value was 2.3 nm. This thickness is close to or slightly smaller than the calculated molecular length of C_{16}TAC with the extended alkyl chain [33]. Thus, in contrast to the assumed additional adsorption on the monolayer, the consistency of the adlayer thickness with the molecular length indicates the formation of the interdigited structure by C_{16}TAC molecules adsorbed on MPA SAM, as illustrated in Fig. 7. This adsorption scheme is reasonable, if the arrangement of MPA molecules in SAM is not compact.

In situ adsorption of C_{16}TAC on 1-dodecanethiol SAM has been examined by SPR spectroscopy [23]. At medium concentrations such as $(0.5\text{–}10)\times10^{-3}$ wt%, the resonance angle shift displays a maximum at early adsorption times and reaches a constant value after longer times. This profile cannot be explained by additional adsorption on monolayer, but indicates the rearrangement and desorption of molecules initially adsorbed.

The computer-simulated curve, based on a modified version of Eq. (2.23),

$$I'_{\Delta\mathrm{angle}} = I'_{\Delta\mathrm{angle},1}\left\{1 - \exp(-k'_{1,\mathrm{obs}}t)\right\} + I'_{\Delta\mathrm{angle},2}\left\{1 - \exp(-k'_{2,\mathrm{obs}}t)\right\}, \tag{3.3}$$

is shown in Fig. 8, and it is compared with the observed one. In Eq. (3.3), $I'_{\Delta\mathrm{angle}}$ is the SPR reflection angle shift. The optimum parameters of the fitting were $I'_{\Delta\mathrm{angle},1} = 0.023°$,

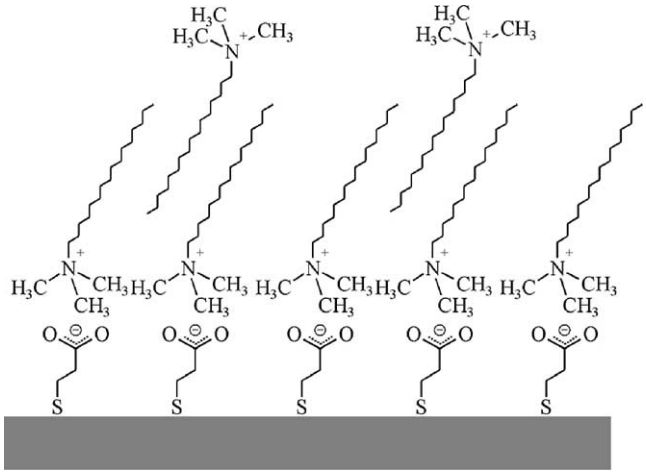

Fig. 7. Model of C_{16}TAC adsorption on MPA SAM.

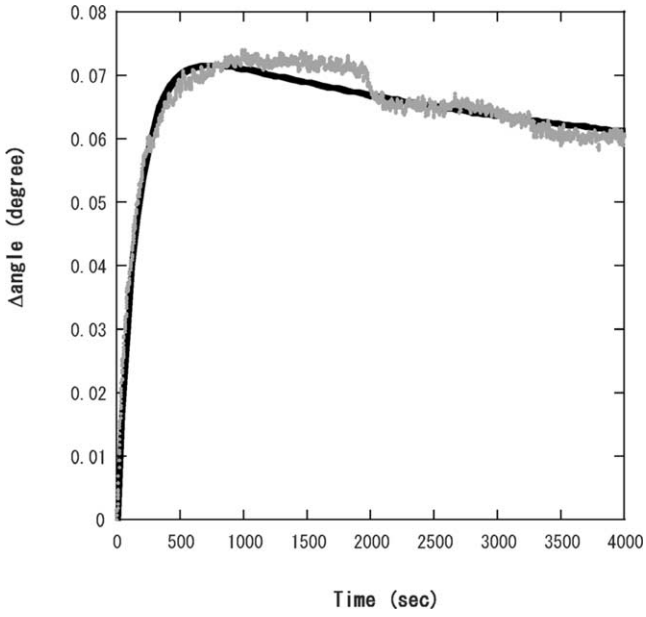

Fig. 8. SPR reflectance angle shift as a function of adsorption time for C_{16}TAC adsorption from an aqueous 0.005 wt% solution on 1-dodecanethiol SAM [23] and the corresponding computer simulation. Gray line, obs; black line, the curve calculated from Eq. (3.3), on the basis of the mechanism in Fig. 4, with $I'_{\Delta\text{angle},1} = 0.023°$, $k'_{1,\text{obs}} = 0.00029\ \text{s}^{-1}$, $I'_{\Delta\text{angle},2} = 0.077°$, and $k'_{2,\text{obs}} = 0.006\ \text{s}^{-1}$ (correlation coefficient 0.972).

$k'_{1,\text{obs}} = 0.00029\ \text{s}^{-1}$, $I'_{\Delta\text{angle},2} = 0.077°$, and $k'_{2,\text{obs}} = 0.006\ \text{s}^{-1}$.

The agreement of the fitting indicates that on a hydrophobic SAM, such as 1-dodecanethiol SAM, excess C_{16}TAC molecules are easy to adsorb at the early stage. However, the excess molecules rearrange to be a monolayer by the hydrophobic interaction with SAM, as illustrated in Fig. 9. This is the reasonable adsorption process observed for amphiphilic molecules on hydrophobic substrates, since the resultant hydrophilic surface faces the bulk solution at the equilibrium state of the adsorption.

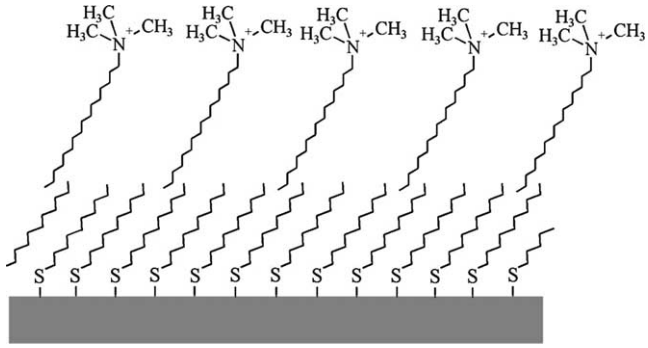

Fig. 9. Model of C_{16}TAC adsorption on 1-dodecanethiol SAM.

4. Conclusions

In the present work, new kinetics equations were derived for two kinds of adsorption mechanisms. On the first mechanism, the surface coverage by the adsorbed molecules increases relatively rapid at early stage due to the formation of first adlayer and then gradually at longer time scale by the formation of the second adlayer. The total coverage depends on the degree of the contribution of two adsorption processes. On the other hand, on the second mechanism, the maximum coverage happens by the excess adsorption at the early stage. The excess molecules are desorbed at the long time scale, accompanying with the rearrangement to the monolayer. It has been shown that, for the adsorption of the cationic surfactant, C_{16}TAC, the adsorption kinetics on anionic and hydrophobic SAMs obeys the former and latter mechanisms, respectively. Computer-simulated curves, obtained on the basis of the assumed mechanisms, satisfactorily reproduced the observed ones.

Some adsorption kinetics reported in the literature does not obey the Langmuir adsorption kinetics. The equations derived in the present paper could be applied to some of such cases with a reasonable physical background and a quantitative analysis of the adsorption curves. Observed non-Langmuir adsorption kinetics are almost noncontradictory to the two exponential equations. However, one must know that the physical meaning of the two exponential terms depends on the estimated adsorption mechanism. Thus our strict mathematical developments presented in this work are demanded to specify the physical meaning of the kinetic parameters. Recent development of methodology for adsorption kinetics will bring more complicated data, especially of non-Langmuir adsorption kinetics, and impose more quantitative and strict analyses of the kinetic data.

Appendix A

The Laplace transformation of differential calculus is

$$\mathcal{L}\big[f'(t)\big] = \int_0^\infty f'(t)e^{-pt}\,dt$$

$$= \big[f(t)e^{-pt}\big]_0^\infty + p\int_0^\infty f(t)e^{-pt}\,dt$$
$$= p\mathcal{L}\big[f(t)\big] - f(0). \tag{A.1}$$

The linearity of Laplace transformation for $f(t) = f_1(t) + f_2(t) + \cdots + f_n(t)$ is given as

$$\mathcal{L}\big[f(t)\big] = \int_0^\infty \big[f_1(t) + f_2(t) + \cdots + f_n(t)\big]e^{-pt}\,dt$$
$$= \int_0^\infty f_1(t)e^{-pt}\,dt + \int_0^\infty f_2(t)e^{-pt}\,dt + \cdots + \int_0^\infty f_n(t)e^{-pt}\,dt$$
$$= \mathcal{L}\big[f_1(t)\big] + \mathcal{L}\big[f_2(t)\big] + \cdots + \mathcal{L}\big[f_n(t)\big]. \tag{A.2}$$

The formula of Laplace transformation is

$$\mathcal{L}[1] = \int_0^\infty e^{-pt}\,dt = \frac{1}{p}, \tag{A.3}$$

$$\mathcal{L}^{-1}\left[\frac{1}{p}\right] = \begin{cases} 0 & (t<0), \\ 1 & (t\geqslant 0), \end{cases} \tag{A.4}$$

$$\mathcal{L}^{-1}\left[\frac{1}{p^2}\right] = t, \tag{A.5}$$

$$\mathcal{L}^{-1}\left[\frac{p}{p^2+2ap+b^2}\right] = \frac{1}{2\sqrt{a^2-b^2}}\Big[\big(a+\sqrt{a^2-b^2}\big)\exp\big\{-\big(a+\sqrt{a^2-b^2}\big)t\big\} - \big(a-\sqrt{a^2-b^2}\big)\exp\big\{-\big(a-\sqrt{a^2-b^2}\big)t\big\}\Big]. \tag{A.6}$$

The Laplace retransformation of the product is

$$\mathcal{L}^{-1}\big[F(p)G(p)\big] = \int_0^t f(t-\tau)g(\tau)\,d\tau.$$

Here

$$\mathcal{L}^{-1}\big[F(p)\big] = f(t) \quad \text{and} \quad \mathcal{L}^{-1}\big[G(p)\big] = g(t). \tag{A.7}$$

Appendix B

If Eqs. (2.8) and (2.9) are Laplace transformed using Eqs. (A.1)–(A.3) and the initial condition is imposed,

$$p\mathcal{L}[N_1] = \frac{k_a C N}{p} - (k_a C + k_d)\mathcal{L}[N_1] + k_d\mathcal{L}[N_2], \tag{B.1}$$

$$p\mathcal{L}[N_2] = k'_a C\mathcal{L}[N_1] - (k'_a C + k'_d)\mathcal{L}[N_2]. \tag{B.2}$$

Then $\mathcal{L}[N_1]$ calculated from Eqs. (B.1) and (B.2) is

$$\mathcal{L}[N_1] = \frac{k_a C N(p+k'_a C+k'_d)}{p\{p^2+(k_a C+k_d+k'_a C+k'_d)p+k_a k'_a C^2+k_a k'_d C+k_d k'_d\}}. \tag{B.3}$$

From the definitions given in (2.14), Eq. (B.3) becomes

$$\mathcal{L}[N_1] = \frac{\delta(p+\gamma)N}{p(p^2+2\alpha p+\beta^2)} = \left(\frac{\delta}{p}+\frac{\delta\gamma}{p^2}\right)\left(\frac{p}{p^2+2\alpha p+\beta^2}\right)N. \tag{B.4}$$

Define that

$$F(p) \equiv \left(\frac{\delta}{p}+\frac{\delta\gamma}{p^2}\right)N, \tag{B.5}$$

$$G(p) \equiv \left(\frac{p}{p^2+2\alpha p+\beta^2}\right), \tag{B.6}$$

and assume that $f(t)$ and $g(t)$ are Laplace retransformations of $F(p)$ and $G(p)$, respectively. Then

$$f(t) = (\delta+\delta\gamma t)N \tag{B.7}$$

and

$$g(t) = \frac{1}{2\sqrt{\alpha^2-\beta^2}} \times \Big[\big(\alpha+\sqrt{\alpha^2-\beta^2}\big)\exp\big\{-\big(\alpha+\sqrt{\alpha^2-\beta^2}\big)t\big\} - \big(\alpha-\sqrt{\alpha^2-\beta^2}\big)\exp\big\{-\big(\alpha-\sqrt{\alpha^2-\beta^2}\big)t\big\}\Big] \tag{B.8}$$

from Eqs. (A.4)–(A.6). If $X = \alpha+\sqrt{\alpha^2-\beta^2}$ and $Y = \alpha-\sqrt{\alpha^2-\beta^2}$, Eq. (B.8) is replaced by

$$g(t) = \frac{1}{X-Y}\big[X\exp(-Xt) - Y\exp(-Yt)\big]. \tag{B.9}$$

If the Laplace retransformation of Eq. (B.4) is performed using Eq. (A.7),

$$\mathcal{L}^{-1}\big[F(p)G(p)\big] = \int_0^t \delta\big\{1+\gamma(t-\tau)\big\} \times \left[\frac{1}{X-Y}\big\{X\exp(-X\tau) - Y\exp(-Y\tau)\big\}\right]N\,d\tau$$
$$= \frac{\delta N}{X-Y}\left[(1+\gamma t) \times \left\{X\int_0^t \exp(-X\tau)\,d\tau - Y\int_0^t \exp(-Y\tau)\,d\tau\right\} - \gamma\left\{X\int_0^t \tau\exp(-X\tau)\,d\tau - Y\int_0^t \tau\exp(-Y\tau)\,d\tau\right\}\right]. \tag{B.10}$$

Now

$$X\int_0^t \exp(-X\tau)\,d\tau - Y\int_0^t \exp(-Y\tau)\,d\tau = X\left[-\frac{1}{X}\exp(-X\tau)\right]_0^t - Y\left[-\frac{1}{Y}\exp(-Y\tau)\right]_0^t = -\exp(-Xt) + \exp(-Yt) \tag{B.11}$$

and

$$X\int_0^t \tau\exp(-X\tau)\,d\tau - Y\int_0^t \tau\exp(-Y\tau)\,d\tau$$
$$= X\left[-\frac{\exp(-X\tau)}{X^2}(X\tau+1)\right]_0^t - Y\left[-\frac{\exp(-Y\tau)}{Y^2}(Y\tau+1)\right]_0^t$$
$$= -t\{\exp(-Xt)-\exp(-Yt)\} - \frac{1}{X}\exp(-Xt) + \frac{1}{Y}\exp(-Yt) + \frac{1}{X} - \frac{1}{Y}. \quad \text{(B.12)}$$

If Eqs. (B.11) and (B.12) are substituted into Eq. (B.10),

$$\mathcal{L}^{-1}[F(p)G(p)] = \frac{\delta N}{X-Y}\left[(1+\gamma t)\{-\exp(-Xt)+\exp(-Yt)\} - \gamma\left\{-t\{\exp(-Xt)-\exp(-Yt)\} - \frac{1}{X}\exp(-Xt) + \frac{1}{Y}\exp(-Yt) + \frac{1}{X} - \frac{1}{Y}\right\}\right]$$
$$= \frac{\delta N}{X-Y}\left[\frac{X-Y}{XY}\gamma + \frac{\gamma-X}{X}\exp(-Xt) - \frac{\gamma-Y}{Y}\exp(-Yt)\right]. \quad \text{(B.13)}$$

Finally,

$$N_1 = \frac{\gamma\delta N}{XY} + \frac{\delta N}{X-Y}\left\{\frac{\gamma-X}{X}\exp(-Xt) - \frac{\gamma-Y}{Y}\exp(-Yt)\right\}. \quad \text{(B.14)}$$

On the other hand, from Eq. (B.2),

$$\mathcal{L}[N_2] = \frac{k_a' C}{p + k_a' C + k_d'}\mathcal{L}[N_1] = \frac{\delta'}{p+\gamma}\mathcal{L}[N_1]. \quad \text{(B.15)}$$

When Eq. (B.4) is substituted into Eq. (B.15),

$$\mathcal{L}[N_2] = \frac{\delta\delta' N}{p(p^2+2\alpha p+\beta^2)}. \quad \text{(B.16)}$$

After the Laplace retransformation of Eq. (B.16),

$$N_2 = \frac{\delta\delta' N}{XY} + \frac{\delta\delta' N}{X-Y}\left\{\frac{1}{X}\exp(-Xt) - \frac{1}{Y}\exp(-Yt)\right\}. \quad \text{(B.17)}$$

References

[1] C.D. Bain, E.B. Troughton, Y.-T. Tao, J. Evall, G.M. Whitesides, R.G. Nuzzo, J. Am. Chem. Soc. 111 (1989) 321.
[2] H.A. Biebuyck, C.D. Bain, G.M. Whitesides, Langmuir 10 (1994) 1825.
[3] N. Garg, J.M. Friedman, T.R. Lee, Langmuir 16 (2000) 4266.
[4] F. Auer, B. Sellergren, A. Swietlow, A. Offenhäuser, Langmuir 16 (2000) 5936.
[5] F. Auer, M. Scotti, A. Ulman, R. Jordan, B. Sellergren, J. Garno, G. Liu, Langmuir 16 (2000) 7554.
[6] C.W. Meuse, Langmuir 16 (2000) 9483.
[7] K. Shimizu, I. Yag, Y. Sato, K. Uosaki, Langmuir 8 (1992) 1385.
[8] D.S. Karpovich, G.J. Blanchard, Langmuir 10 (1994) 3315.
[9] W. Pan, C.J. Durning, N.J. Turro, Langmuir 12 (1996) 4469.
[10] K. Matsuura, A. Tsuchida, Y. Okahata, T. Akaike, K. Kobayashi, Bull. Chem. Soc. Jpn. 71 (1998) 2973.
[11] C.H. Kim, S.W. Han, T.H. Ha, K. Kim, Langmuir 15 (1999) 8399.
[12] T. Hasegawa, K. Matsuura, K. Ariga, K. Kobayashi, Macromolecules 33 (2000) 2772.
[13] Z. Tang, S. Liu, E. Wang, S. Dong, Langmuir 16 (2000) 4946.
[14] K.A. Peterlinz, R. Georgiadis, Langmuir 12 (1996) 4731.
[15] L.M. Williams, S.D. Evans, T.M. Flynn, A. Marsh, P.F. Knowles, R.J. Bushby, N. Boden, Langmuir 13 (1997) 751.
[16] J. Lahiri, L. Isaacs, B. Grzybowski, J.D. Carbeck, G.M. Whitesides, Langmuir 15 (1999) 7186.
[17] S. Schouten, P. Stroeve, M.L. Longo, Langmuir 15 (1999) 8133.
[18] L. Zhang, M.L. Longo, P. Stroeve, Langmuir 16 (2000) 5093.
[19] J. Lahiri, P. Kalal, A.G. Frutos, S.J. Jonas, R. Schaeffler, Langmuir 16 (2000) 7805.
[20] L.S. Jung, K.E. Nelson, P.S. Stayton, C.T. Campbell, Langmuir 16 (2000) 9421.
[21] Y.-Y. Luk, M. Kato, M. Mrksich, Langmuir 16 (2000) 9604.
[22] T. Imae, M. Ito, K. Aoi, K. Tsutsumiuchi, H. Noda, M. Okada, Colloid Surf. A Physicochem. Eng. Aspects 175 (2000) 225.
[23] T. Imae, T. Takeshita, K. Yahagi, Stud. Surf. Sci. Catal. 132 (2001) 477.
[24] E.S. Pagac, D.C. Prieve, R.D. Tilton, Langmuir 14 (1998) 2333.
[25] R. Atkin, V.S. Craig, S. Biggs, Langmuir 16 (2000) 9374.
[26] K. Hu, A.J. Bard, Langmuir 14 (1998) 4790.
[27] S. Xu, S.J.N. Cruchon-Dupeyrat, J.C. Garno, G.-Y. Liu, J. Chem. Phys. 108 (1998) 5002.
[28] D.J. Lavrich, S.M. Wetterer, S.L. Bernasek, G. Scoles, J. Phys. Chem. B 102 (1998) 3456.
[29] K. Takada, G.D. Storrier, M. Morán, H.D. Abruña, Langmuir 15 (1999) 7333.
[30] I.C. Stefan, D.A. Scherson, Langmuir 16 (2000) 5945.
[31] T. Imae, H. Torii, J. Phys. Chem. B 104 (2000) 9218.
[32] T. Imae, N. Yoshida, unpublished data.
[33] C. Tanford, The Hydrophobic Effect, Wiley, New York, 1980.